Photocatalysis Hot Paper

DOI: 10.1002/anie.201405161

Harvesting Solar Light with Crystalline Carbon Nitrides for Efficient Photocatalytic Hydrogen Evolution**

*Manas K. Bhunia, Kazuo Yamauchi, and Kazuhiro Takanabe**

Abstract: *Described herein is the photocatalytic hydrogen evolution using crystalline carbon nitrides (CNs) obtained by supramolecular aggregation followed by ionic melt polycondensation (IMP) using melamine and 2,4,6-triaminopyrimidine as a dopant. The solid state NMR spectrum of ^{15}N-enriched CN confirms the triazine as a building unit. Controlling the amount and arrangements of dopants in the CN structure can dramatically enhance the photocatalytic performance for H_2 evolution. The polytriazine imide (PTI) exhibits the apparent quantum efficiency (AQE) of 15% at 400 nm. This method successfully enables a substantial amount of visible light to be harvested for H_2 evolution, and provides a promising route for the rational design of a variety of highly active crystalline CN photocatalysts.*

Producing hydrogen, an environmentally benign energy carrier with a high energy density, from water splitting is a primary goal of modern chemistry.[1] The rational design and synthesis of abundant, sustainable, and efficient metal-free photocatalytic materials that operate with visible light continue to be challenges in this field. Recently, the polymeric carbon nitride (CN) semiconductor g-C_3N_4 has attracted significant attention because this catalyst exhibited stable performance in the photocatalytic water-splitting reaction (half reaction) under visible light.[2] The semiconductor properties of g-C_3N_4 result from the formation of an extended π-conjugated system from s-triazine units and largely rely on the extent of their polymerization. A structural characterization revealed the presence of unreacted amino and/or cyano functionalities owing to incomplete polymerization.[3] During photocatalysis, these residual functionalities often act as electron trap sites, whereas the presence of an optimum number of non-radiative defects/recombination centers enhances photocatalytic activity.[4] The photocatalytic properties are sensitively affected by the crystallinity of the photocatalyst. Constructing crystalline photocatalyst with reduced trap-site density that works under visible-light is thus a promising but challenging task.

To extend the visible-light response and to improve the hydrogen evolution reaction (HER) activity, numerous modifications in the synthesis of CNs have been explored, including the incorporation of barbituric acid,[5] molecules with heteroatoms,[6] dopants,[7] and semiconductors,[8] as well as producing thin sheets through exfoliation.[9] In photocatalysis, the directional flow of electrons largely depends on the organization of the molecules in the structure in relation to their crystallinity. Supramolecular assembly of CN precursors can give a better arrangement through hydrogen bonding as it causes the molecules to align in a particular order.[10,11] But their solid-state synthesis at high temperature is limited with the immobility of the reaction intermediates that leads to incomplete polymerization and produces amorphous materials. Ionothermal synthesis can offer a more appropriate solvent for the CN precursors.[12,13] Recently, Lotsch et al. reported amorphous CN material even though they employed ionothermal synthesis.[14] Thus, it is essential to develop new strategies for the rational synthesis of CN photocatalysts to further improve their crystallinity and photocatalytic efficiencies.

In this study, we prepared a crystalline triazine-based CN by employing chemically compatible organic molecules to circumvent residual functionality. Herein, 2,4,6-triaminopyrimidine (TAP), a member of the nucleobase family, is of particular interest because it has a higher carbon content and its structural features parallel to those of melamine (Mel), a planar molecule with amino groups at each vertex (Scheme 1). By incorporating a subtle amount of this pyrimidine moiety into the CN structure resulted in substantial light harvesting in the visible range. Furthermore, by combining supramolecular aggregation and ionic melt polycondensation, we controlled the degree of crystallinity along with the arrangement of defects in the structure. This two-step rearrangement process together with the controlled amount of the pyrimidine moiety dopant results in the most active triazine-based photocatalysts for HER reported to date.

Experimentally, we synthesized a series of CN supramolecular precursors by varying the amount of TAP added to Mel in absolute ethanol followed by stirring at 100 °C overnight, which afforded a solid crystalline product which were denoted as PrePTI-X (where X is the TAP molar ratio relative to one mole Mel: 0.06, 0.13, 0.25, and 0.5; see Supporting information). The high crystallinity is reflected in the X-ray diffraction (XRD) patterns of the supramolecular complexes of the PTI precursors (Figure S1 in the Supporting

[*] Dr. M. K. Bhunia, Prof. K. Takanabe
Division of Physical Sciences and Engineering
KAUST Catalysis Center (KCC)
King Abdullah University of Science and Technology (KAUST)
4700 KAUST, Thuwal, 23955-6900 (Saudi Arabia)
E-mail: kazuhiro.takanabe@kaust.edu.sa
Dr. K. Yamauchi
Imaging and Characterization Core Lab
King Abdullah University of Science and Technology (KAUST)
4700 KAUST, Thuwal, 23955-6900 (Saudi Arabia)

[**] The research reported in this publication was supported by the King Abdullah University of Science and Technology. Dr. Dalaver H. Anjum and Mr. Shuo Liu are acknowledged for TEM and SEM measurements, respectively.

Supporting information for this article is available on the WWW under http://dx.doi.org/10.1002/anie.201405161.

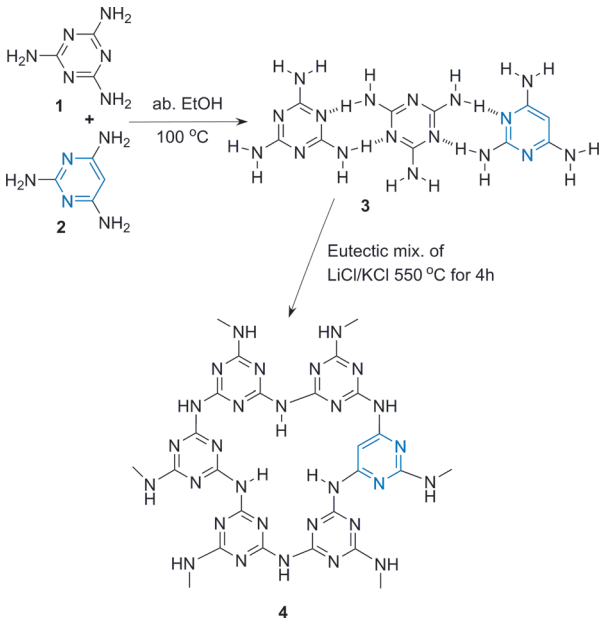

Scheme 1. Scheme for the formation of the PTI samples (the intercalation of Li and Cl is omitted for clarity). Mel (**1**), TAP (**2**), supramolecular aggregation (→**3**), and final proposed PTI structure (**4**).

Information). The appearance of new peaks compared to Mel and TAP, at 20.8° and 33.9°, for the PTI precursor complexes is strong evidence for the creation of a new arrangement. The infrared (IR) spectra (attenuated total reflection mode) shown in Figure S2 provide further evidence for the formation of supramolecular complexes of the PTI precursors. The signal attributed to the aromatic C–C bond is discernible at 1240 cm^{-1} in the spectra of the supramolecular aggregates.

These supramolecular aggregates were then mixed with a eutectic mixture of LiCl and KCl and heated at 550 °C. The samples obtained were denoted PTI-X. As a prototype crystalline CN, PTI/LiCl was synthesized using a slight modification of our previous method,[13b] and was denoted as PTI-0.

The XRD pattern of PTI-0 matched well to that of the crystalline CN reported by Wirnhier et al.[13a] (Figure 1 a). For the doped sample, a new small peak at 14.2°, close to the 12.1° reflection peak attributable to the in-plane arrangements of N-linked heterocyclic rings, becomes more prominent as the dopant concentration increases. At higher concentrations of dopant, both of these peaks disappear, presumably because of disturbances in packing and potential modifications in the single layers. The predominant (002) peak at 27.1° corresponding to the interlayer stacking distance of 3.29 Å for PTI-0.13 broadens as the concentration of dopant increases, reflecting the structural disorder. The (002) peak in the doped samples shifts to slightly higher angles compared to undoped PTI-0 ($d = 3.35$ Å), indicating contraction of the interlayer. Typical TEM image analysis together with the diffraction pattern of the PTI-0.13 supports its crystallinity (Supporting Information).

Furthermore, the IR bands in Figure 1 b become broader as the concentration of dopant increases, although the peak at 805 cm^{-1}, attributable to the triazine ring breathing mode, is discernible in all of the samples, which indicates that the order of the molecules is destroyed. The peaks representing the ring deformation appear at 1576 and 1445 cm^{-1}. The fingerprint region between 1200 and 1620 cm^{-1}, which is assigned as stretching vibrations of heterocyclic CN, is noticeable. The bands at 1269 and 740 cm^{-1}, which are attributed to the presence of C-NH-C stretching and bending vibrations in the PTI-0, respectively, are broadened and shifted to the lower wavenumber region in the doped samples. The new peak at 912 cm^{-1}, corresponding to the aromatic C–H out-of-plane bending vibration, further supports the presence of pyrimidine in the CN structure.

Elemental analyses (EA) clearly reveal that the C/N molar ratio increases with the increase in dopant concentration (Table 1). Typically, the C/N ratio is 0.66 for undoped PTI-0, whereas it increases to 0.73 for PTI-0.13. Thus, the IR and elemental analysis results clearly indicate the incorporation of C atoms, through the integration of the pyrimidine moiety, into the CN. The inductively coupled plasma atomic emission spectroscopy (ICP-AES) measurement revealed that the amount of Li was less in the doped samples than in the PTI-0, which was consistent with their electron energy-loss spectra (EELS) shown in the Supporting Information.

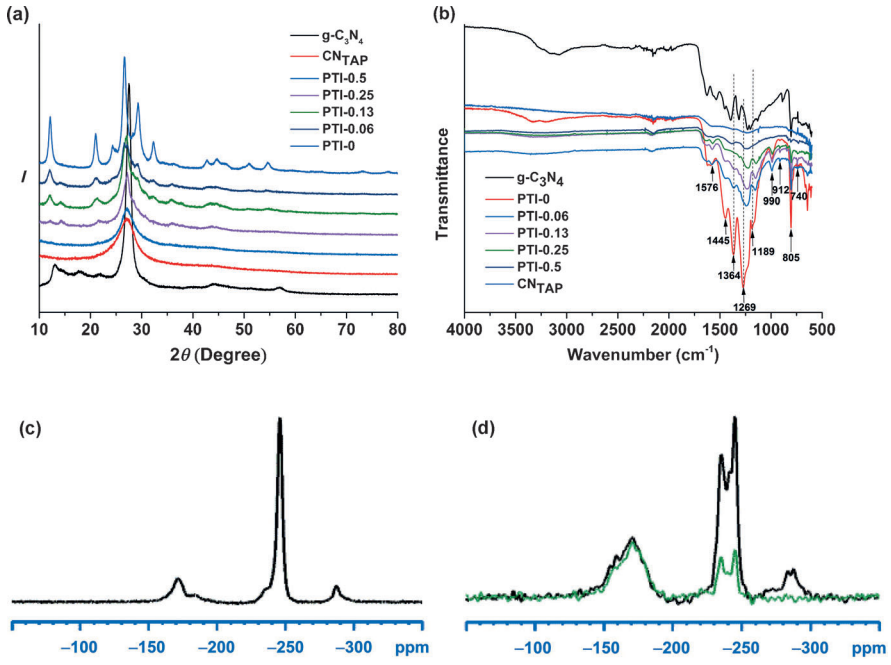

Figure 1. a) Powder XRD pattern, b) IR spectra, c) solid-state ^{15}N CP MAS NMR spectrum of ^{15}N-enriched PTI-0, and d) solid state ^{15}N CP MAS NMR spectrum (black) and ^{15}N CPPI MAS NMR spectrum (green) of ^{15}N-enriched PTI-0.13.

Table 1: Physicochemical properties of carbon nitrides.

Sample	Mel:TAP [mol ratio]	C/N [mol ratio]	SA[a] [$m^2 g^{-1}$]	HER[b] [$\mu mol\, h^{-1}$]
g-C_3N_4	1:0	0.65	10	15
PTI-0	1:0	0.66	90	22
PTI-0.06	1:0.06	0.70	119	185
PTI-0.13	1:0.13	0.73	93	204
PTI-0.25	1:0.25	0.78	26	62
PTI-0.5	1:0.5	0.87	12	4
CN_{TAP}	0:1	1.12	8	–

[a] BET surface area; [b] HER rate in the first hour of the reaction over the samples (25 mg) loaded with 3 wt% Pt in 10 vol% TEOA/water solution under visible light irradiation ($\lambda > 420$ nm).

Solid-state ^{13}C and ^{15}N CP MAS NMR spectra of PTI-0.13 provide additional structural insight. As shown in Figure 1d and Figure S3, the spectra were well resolved, reflecting the nanocrystallinity of the material, which points to an improved condensation and local organization in the structure. A very strong signal at approximately $\delta = 162$ ppm in the ^{13}C CP MAS NMR spectrum of PTI-0.13 is attributed to the characteristic peak of the ring carbon of the triazine or heptazine moiety. The ^{15}N CP MAS NMR spectrum of the ^{15}N-enriched PTI-0.13 (Figure 1d) has two broad peaks at $\delta = -170$ and -287 ppm, attributable to tertiary nitrogen and primary amine, respectively, as well as two well-resolved distinct peaks at $\delta = -236$ and -245 ppm, which might be due to the presence of two different bridging NH chemical environments present in the CN structure compared to that of PTI-0 (cf. Figure 1c). To determine whether the building unit is triazine or heptazine, we performed ^{15}N cross-polarization polarization inversion (CPPI) MAS NMR measurements of the ^{15}N-enriched PTI-0.13 sample with an inversion time of 400 μs. The resulting spectra showed lower intensities of the NH signals, whereas the signal for the tertiary nitrogen atoms remained unaffected (Figure 1d). This result explicitly confirms the presence of triazine building blocks instead of heptazine units.[15]

The strongest indication of doping can be observed from the color change of the samples, and the DR UV/Vis spectra of the samples are shown in Figure 2. The color of the undoped PTI-0 is yellow, whereas the color changes to brownish yellow, brown, and then deep brown for the samples with increased concentrations of dopant from PTI-0.06 to PTI-0.5. These color changes are consistent with the red shift observed in the sample's absorption spectra. For g-C_3N_4, the absorption band typically appears in the blue part of the visible region.[2] When the dopant concentration increases, the absorption band gradually expands to the visible wavelength region. The increase in the number of dopants,[7] and/or the increased π-electron delocalization in the conjugated system[16] might be a plausible reason for the enhanced light harvesting in the visible region.[17]

A visible light-induced hydrogen-evolution assay was conducted on the CN samples (25 mg) in the presence of 3 wt% Pt as a co-catalyst and triethanolamine (TEOA) as a sacrificial electron donor (Table 1). The photocatalytic HER rate of the crystalline PTI-0 was 22 $\mu mol\, h^{-1}$, which is

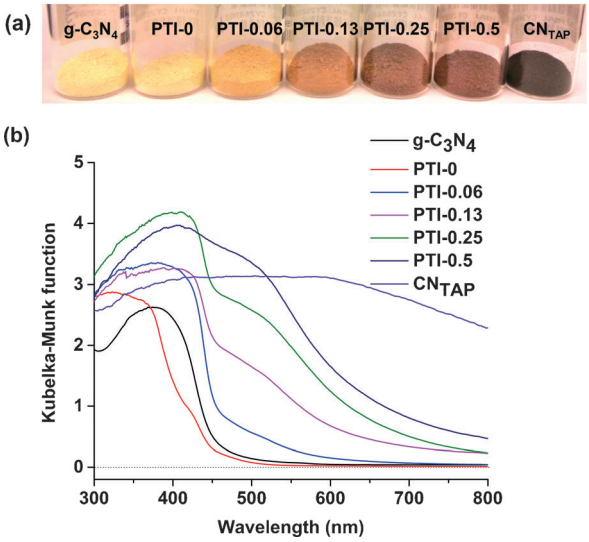

Figure 2. a) Color of the samples, b) UV/Vis diffuse reflectance spectra of the carbon nitrides.

higher than that of g-C_3N_4 (15 $\mu mol\, h^{-1}$). Of the doped PTI samples, the initial HER rate for PTI-0.13 was observed to be the highest, 204 $\mu mol\, h^{-1}$, which is a factor of 14-times greater than that of g-C_3N_4. The apparent quantum efficiency (AQE) of the PTI-0.13 was approximately 7.0% at 420 nm. The initial HER rate for PTI-0.06 was 185 $\mu mol\, h^{-1}$; however, increasing the concentration of dopant beyond PTI-0.13 results in lower activity.

The introduction of dopant can increase the HER activity, while the optimum ratio of dopant is related to the ideal optoelectronic situation that allows the catalyst to carry out photocatalytic activity. Notably, the HER rate of PTI-0.5 was only 4 $\mu mol\, h^{-1}$ when the CN structure was seriously deconstructed as the dopant concentration increased (as evidenced from the IR and powder XRD data), which supports our hypothesis that the optimum ratio of triazines to pyrimidine together with their perfect organization, in particular, the in-plane arrangement of these moieties in the surface, is the key factor in achieving higher photocatalytic HER activity. We successfully demonstrated this concept by examining the photocatalytic activities of a series of samples (CN-0.13) that possessed the same concentration ratio as that of PTI-0.13 (Table S2) but were synthesized using varying reaction methods. Initially, we prepared CN-0.13_g by simple grinding and heating. Then, CN-0.13_{gf} was prepared by grinding with a eutectic mixture of ionic salts followed by heating. Finally, CN-0.13_s was prepared by mixing with ethanol, drying, and heating without ionic salts. Intriguingly, the PTI-0.13 sample exhibited HER activity that was at least a factor of two greater than the HER activities of the other CN-0.13 analogues (Figure 3a).

The solvent ethanol not only has an effect on the reorganization of the precursors but also contributes to the photophysical properties of the resulting CNs.[9] It was reported that the fluorescence lifetime was shortened for the CN prepared from the supramolecular aggregation of cyanuric acid and Mel in ethanol compared to that prepared

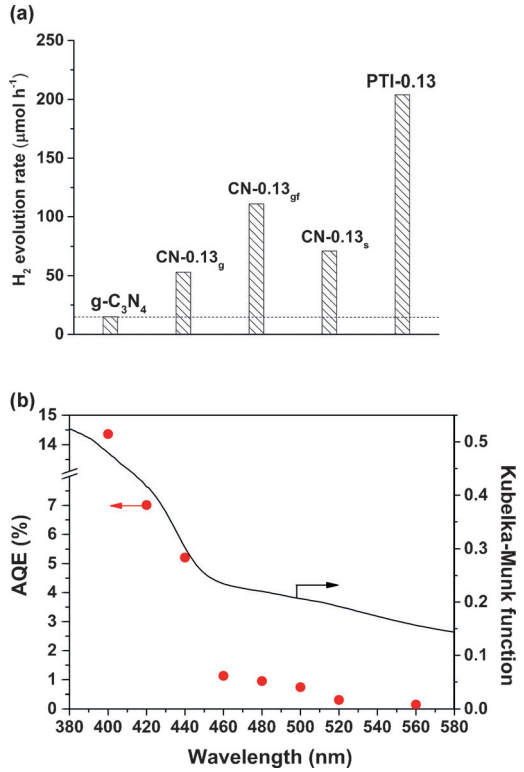

Figure 3. a) Photocatalytic HER rates of the CN samples prepared using different methods (see text for details) b) wavelength-dependent AQE of H_2 evolution over 3 wt% Pt/PTI-0.13 (left axis), DR UV/Vis spectrum of PTI-0.13 (right axis).

in chloroform, which indicates the involvement of a new charge-transfer process.[11] To investigate the effect of the surface area (SA) on the photocatalytic activity,[18] N_2 adsorption/desorption measurements of the catalysts were performed. In Table 1, from the measured BET specific SAs, it is difficult to form a correlation between activity and SA. The TEM image of the PTI-0.13 after photocatalytic reaction for 15 h clearly shows the finely dispersed Pt nanoparticles of approximate size 11.2 nm on the exterior of the CN nanoparticles (Supporting Information).

It is instructive to know which wavelength actively contributes to the HER. To determine this wavelength, wavelength-dependent hydrogen evolution for PTI-0.13 was examined using monochromatic light. As shown in Figure 3b, the AQE of the HER was the highest at a wavelength of 400 nm, while the AQE then decreased beginning at 420 nm. Though the main contribution to the HER comes from the photons below the 450 nm wavelength regions, the AQE trend line spans to the higher wavelengths, indicating that the extended visible-light absorption indeed contributes to the photocatalytic HER. This decreased photocatalytic efficiency in the extended range of visible-light is likely associated with the localized electronic states originating from dopant levels of TAP molecules within those of the pristine PTI polymer.

In conclusion, through active control of the number and arrangement of pyrimidine moieties, or defects, in CN materials, we successfully harvested a substantial amount of visible-light and very efficiently utilized it for the HER from an aqueous triethanolamine solution. The improved structure condensation provides high crystallinity, evidenced by powder XRD and TEM analysis, and remarkably increased HER rate, reaching AQE of approximately 7% at 420 nm, which is the highest value for triazine-based CNs. The two-step rearrangement process, supramolecular aggregation and ionic melt polycondensation, together with controlled modification of the chemically compatible dopant, might be a promising route for the rational design of a variety of active crystalline CN photocatalysts from a diverse range of inexpensive, organic CN precursors.

Received: May 10, 2014
Published online: August 14, 2014

Keywords: carbon nitride · hydrogen evolution · photocatalysis · semiconductors · solar-energy conversion

[1] a) J. A. Turner, *Science* **2004**, *305*, 972 – 974; b) N. S. Lewis, D. G. Nocera, *Proc. Natl. Acad. Sci. USA* **2006**, *103*, 15729 – 15735; c) A. Kudo, Y. Miseki, *Chem. Soc. Rev.* **2009**, *38*, 253 – 278; d) F. E. Osterloh, *Chem. Soc. Rev.* **2013**, *42*, 2294 – 2320; e) U. Eberle, M. Felderhoff, F. Schüth, *Angew. Chem.* **2009**, *121*, 6732 – 6757; *Angew. Chem. Int. Ed.* **2009**, *48*, 6608 – 6630; f) H. Vrubel, T. Moehl, M. Grätzel, X. Hu, *Chem. Commun.* **2013**, *49*, 8985 – 8987.

[2] a) X. C. Wang, K. Maeda, A. Thomas, K. Takanabe, G. Xin, J. M. Carlsson, K. Domen, M. Antonietti, *Nat. Mater.* **2009**, *8*, 76 – 80; b) Y. Wang, X. Wang, M. Antonietti, *Angew. Chem.* **2012**, *124*, 70 – 92; *Angew. Chem. Int. Ed.* **2012**, *51*, 68 – 89.

[3] Z. Lin, X. Wang, *Angew. Chem.* **2013**, *125*, 1779 – 1782; *Angew. Chem. Int. Ed.* **2013**, *52*, 1735 – 1738.

[4] X. B. Chen, L. Liu, P. Y. Yu, S. S. Mao, *Science* **2011**, *331*, 746 – 750.

[5] J. Zhang, X. Chen, K. Takanabe, K. Maeda, K. Domen, J. D. Epping, X. Fu, M. Antonietti, X. Wang, *Angew. Chem.* **2010**, *122*, 451 – 454; *Angew. Chem. Int. Ed.* **2010**, *49*, 441 – 444.

[6] a) J. Zhang, M. Zhang, S. Lin, X. Fu, X. Wang, *J. Catal.* **2014**, *310*, 24 – 30; b) J. Zhang, G. Zhang, X. Chen, S. Lin, L. Mçhlmann, G. Dołęga, G. Lipner, M. Antonietti, S. Blechert, X. Wang, *Angew. Chem.* **2012**, *124*, 3237 – 3241; *Angew. Chem. Int. Ed.* **2012**, *51*, 3183 – 3187.

[7] X.-H. Li, J.-S. Chen, X. Wang, J. Sun, M. Antonietti, *J. Am. Chem. Soc.* **2011**, *133*, 8074 – 8077.

[8] a) Y. Zhang, T. Mori, J. Ye, M. Antonietti, *J. Am. Chem. Soc.* **2010**, *132*, 6294 – 6295; b) H. Kisch, *Angew. Chem.* **2013**, *125*, 842 – 879; *Angew. Chem. Int. Ed.* **2013**, *52*, 812 – 847.

[9] a) S. Yang, Y. Gong, J. Zhang, L. Zhan, L. Ma, Z. Fang, R. Vajtai, X. Wang, P. M. Ajayan, *Adv. Mater.* **2013**, *25*, 2452 – 2456; b) K. Schwinghammer, M. B. Mesch, V. Duppel, C. Ziegler, J. Senker, B. V. Lotsch, *J. Am. Chem. Soc.* **2014**, *136*, 1730 – 1733.

[10] a) C. T. Seto, J. P. Mathias, G. M. Whitesides, *J. Am. Chem. Soc.* **1993**, *115*, 1321 – 1329; b) L. J. Prins, D. N. Reinhoudt, P. Timmerman, *Angew. Chem.* **2001**, *113*, 2446 – 2492; *Angew. Chem. Int. Ed.* **2001**, *40*, 2382 – 2426; c) Y.-S. Jun, J. Park, S. U. Lee, A. Thomas, W. H. Hong, G. D. Stucky, *Angew. Chem.* **2013**, *125*, 11289 – 11293; *Angew. Chem. Int. Ed.* **2013**, *52*, 11083 – 11087; d) Y.-S. Jun, E. Z. Lee, X. Wang, W. H. Hong, G. D. Stucky, A. Thomas, *Adv. Funct. Mater.* **2013**, *23*, 3661 – 3667.

[11] M. Shalom, S. Inal, C. Fettkenhauer, D. Neher, M. Antonietti, *J. Am. Chem. Soc.* **2013**, *135*, 7118 – 7121.

[12] X. Liu, N. Fechler, M. Antonietti, *Chem. Soc. Rev.* **2013**, *42*, 8237 – 8265.

[13] a) E. Wirnhier, M. Döblinger, D. Gunzelmann, J. Senker, B. V. Lotsch, W. Schnick, *Chem. Eur. J.* **2011**, *17*, 3213 – 3221; b) Y. Ham, K. Maeda, D. Cha, K. Takanabe, K. Domen, *Chem. Asian J.* **2013**, *8*, 218 – 224.

[14] K. Schwinghammer, B. Tuffy, M. B. Mesch, E. Wirnhier, C. Martineau, F. Taulelle, W. Schnick, J. Senker, B. V. Lotsch, *Angew. Chem.* **2013**, *125*, 2495 – 2499; *Angew. Chem. Int. Ed.* **2013**, *52*, 2435 – 2439.

[15] a) B. Jürgens, E. Irran, J. Senker, P. Kroll, H. Muller, W. Schnick, *J. Am. Chem. Soc.* **2003**, *125*, 10288 – 10300; b) J. R. Holst, E. G. Gillan, *J. Am. Chem. Soc.* **2008**, *130*, 7373 – 7379; c) A. B. Jorge, D. J. Martin, M. T. S. Dhanoa, A. S. Rahman, N. Makwana, J. Tang, A. Sella, F. Corà, S. Firth, J. A. Darr, P. F. McMillan, *J. Phys. Chem. C* **2013**, *117*, 7178 – 7185; d) S. Y. Chong, J. T. A. Jones, Y. Z. Khimyak, A. I. Cooper, A. Thomas, M. Antonietti, M. J. Bojdys, *J. Mater. Chem. A* **2013**, *1*, 1102 – 1107.

[16] M. G. Debije, J. Piris, M. P. de Haas, J. M. Warman, Ž. Tomović, C. D. Simpson, M. D. Watson, K. Müllen, *J. Am. Chem. Soc.* **2004**, *126*, 4641 – 4645.

[17] A. Du, S. Sanvito, Z. Li, D. Wang, Y. Jiao, T. Liao, Q. Sun, H. Y. Ng, Z. Zhu, R. Amal, C. S. Smith, *J. Am. Chem. Soc.* **2012**, *134*, 4393 – 4397.

[18] a) G. Arrachart, C. Carcel, P. Trens, J. J. E. Moreau, M. W. C. Man, *Chem. Eur. J.* **2009**, *15*, 6279 – 6288; b) Y. Zheng, Y. Jiao, J. Chen, J. Liu, J. Liang, A. Du, W. Zhang, Z. Zhu, C. S. Smith, M. Jaroniec, Q. G. Lu, Z. S. Qiao, *J. Am. Chem. Soc.* **2011**, *133*, 20116 – 20119; c) J. Yang, D. Wang, H. Han, C. Li, *Acc. Chem. Res.* **2013**, *46*, 1900 – 1909; d) J. Zhang, M. Zhang, C. Yang, X. Wang, *Adv. Mater.* **2014**, *26*, 4121 – 4126.

